

# ROSSBY WAVE INSTABILITY AT DEAD ZONE BOUNDARIES IN 3D RESISTIVE MAGNETOHYDRODYNAMICAL GLOBAL MODELS OF PROTOPLANETARY DISKS

WLADIMIR LYRA<sup>1,2,3</sup> AND MORDECAI-MARK MAC LOW<sup>1</sup>

*Draft version*

## ABSTRACT

It has been suggested that the transition between magnetorotationally active and dead zones in protoplanetary disks should be prone to the excitation of vortices via Rossby wave instability (RWI). However, the only numerical evidence for this has come from alpha disk models, where the magnetic field evolution is not followed, and the effect of turbulence is parametrized by Laplacian viscosity. We aim to establish the phenomenology of the flow in the transition in 3D resistive-magnetohydrodynamical models. We model the transition by a sharp jump in resistivity, as expected in the inner dead zone boundary, using the PENCIL CODE to simulate the flow. We find that vortices are readily excited in the dead side of the transition. We measure the mass accretion rate finding similar levels of Reynolds stress at the dead and active zones, at the  $\alpha \approx 10^{-2}$  level. The vortex sits in a pressure maximum and does not migrate, surviving until the end of the simulation. A pressure maximum in the active zone also triggers the RWI. The magnetized vortex that results should be disrupted by parasitical magneto-elliptic instabilities, yet it subsists in high resolution. This suggests that either the parasitic modes are still numerically damped, or that the RWI supplies vorticity faster than they can destroy it. We conclude that the resistive transition between the active and dead zones in the inner regions of protoplanetary disks, if sharp enough, can indeed excite vortices via RWI. Our results lend credence to previous works that relied on the alpha-disk approximation, and caution against the use of overly reduced azimuthal coverage on modeling this transition.

## 1. INTRODUCTION

The formation of planets remains one of the most challenging problems of contemporary astrophysics. The current paradigm in planet formation theory describes a hierarchical growth of solid bodies, from interstellar dust grains to rocky planetary cores (Safronov 1969; Lyttleton 1972; Goldreich & Ward 1973; Youdin & Shu 2002). A particularly difficult phase in the process is the growth from centimeter sized pebbles and meter-sized boulders to planetary embryos the size of our Moon or Mars. Objects in the pebble to boulder range are expected to drift inward extremely rapidly in a protoplanetary disk, so that they would generally fall into the central star well before larger bodies can form by simple accumulation (Weidenschilling 1977; Brauer et al. 2008).

Ways to bypass this problem have focused on inhomogeneities in the flow, in order to trap particles in their migrating path. Cuzzi et al. (2008) proposed a model in which mm-sized particles are trapped in the smallest eddies in the flow, forming “sandpile” planetesimals in the 10-100 km range (though that model has been criticized by Chang & Oishi 2010 and Pan et al. 2011). Particles may also be trapped in mesoscale “zonal flows” (Lyra et al. 2008a; Johansen et al. 2009; Simon et al. 2012) that are local inversions in the angular velocity profile, brought about by spatial variations in magnetic pressure. The particles themselves can give rise to the necessary inhomogeneities, as their migrating stream-

ing flow develops into a traffic-jam instability (Youdin & Shu 2002; Youdin & Goodman 2005; Youdin & Johansen 2007), leading to intense particle clumping (Johansen & Youdin 2007) and subsequent planetesimal formation at the Ceres-mass range (Johansen et al. 2007). It has also been recently proposed that icy planetesimals may form from direct coagulation (Okuzumi et al. 2012) due to the enhanced sticking properties of ices.

Another process has been suggested, that combines several of the advantages (as well as many of the problems) of the scenarios described above, and is the subject of this work. Turbulence in the largest scales of the flow, in the form of large scale vortices, has been independently proposed by Barge & Sommeria (1995) and Tanga et al. (1996) as fast routes for planet formation, for two main reasons. First, vortices are equilibrium solutions of the Navier-Stokes equations, and thus are persistent structures in hydrodynamic flows, as seen in the Great Red Spot of Jupiter, a remarkable high pressure vortex stable since first spotted, over three hundred years ago (Hooke 1665; Cassini 1666)<sup>4</sup>. The second is that the equilibrium is geostrophic, i.e, between the Coriolis force and the pressure gradient force. As solids do not feel the pressure force, the Coriolis force will lead them out of the vortex if cyclonic and into the eye if anticyclonic. As the shear enforces that only anticyclonic vortices persist (Marcus 1993; Adams & Watkins 1995; Bracco et al. 1999; Godon & Livio 1999), this becomes a very effective mechanism to concentrate solid particles (Klahr 2006), as also observed in numerical simulations (Godon & Livio 2000; Johansen et al. 2004; Fromang &

wlyra@jpl.nasa.gov, mordecai@amnh.org

<sup>1</sup> Department of Astrophysics, American Museum of Natural History, 79th Street at Central Park West, New York, NY, 10024, USA

<sup>2</sup> Jet Propulsion Laboratory, California Institute of Technology, 4800 Oak Grove Drive, Pasadena, CA, 91109, USA

<sup>3</sup> NASA Carl Sagan Fellow

<sup>4</sup> The reader is referred to the fascinating account of Falorni (1987) on the history of the discovery of the Spot, where the author debates the claims of primacy to Hooke or Cassini.

Nelson 2005; Inaba & Barge 2006). It was further shown by Lyra et al. (2008b, 2009) that in the limit where turbulence in the vortex core is absent and the fragmentation of particles is ignored, the concentration of solids easily reaches the conditions necessary to gravitationally collapse them into planets.

Nevertheless, as exciting as the vortex hypothesis may be, for a long time no plausible mechanism for the formation and sustenance of such storm systems in disks could be found. It is well known that three-dimensional vortices fall prey to elliptical instabilities (Bayly 1986; Pierrehumbert 1986; Kerswell 2002; Lesur & Papaloizou 2009), a general name given to parasitic instabilities of closed elliptical streamlines (see e.g. the review of Kerswell 2002). Fluids in rigid rotation support a spectrum of stable inertial waves, the simplest ones being circularly polarized transverse plane waves oscillating at twice the base frequency (see e.g. Chandrasekhar 1961). Strain is introduced when the motion passes from circular to elliptical, and some three-dimensional modes find resonance with the underlying strain field. Because of its intrinsic three-dimensional character, the absence of elliptic instability modifies the turbulent energy cascade from direct to inverse in 2D (Batchelor 1969). The result is that the series of viscous mergings that turn small and mesoscale eddies into large vortices in the integral scale is not expected to occur in systems that significantly depart from two-dimensionality. In other words, vortices do not spontaneously develop in three dimensions from initial small scale noise as they do in two dimensions, and must therefore be the result of some instability. Because the Keplerian shear provides stabilization of linear axisymmetric disturbances at all Reynolds numbers (Rayleigh criterion; Strutt 1880, 1916), in non-magnetized disks any such instability must be either non-axisymmetric, non-linear, or rely on a modification of the angular velocity profile to circumvent the stabilizing effect of the shear.

Based on these ideas, two main processes have been proposed for the formation of vortices in disks. One is the non-linear radial convection process that has been referred to as global baroclinic instability (Klahr & Bodenheimer 2003; Klahr 2004), subcritical baroclinic instability (Lesur & Papaloizou 2009; Paardekooper et al. 2010), and simply baroclinic instability (Lyra & Klahr 2011). This shall not be dealt with in this barotropic paper. We will focus here on what has become known as Rossby wave instability (RWI; Lovelace et al. 1999; Li et al. 2000, 2001; Umurhan 2010).

The RWI relies on a modification of the angular velocity profile, brought about by a local extremum of an entropy-modified potential vorticity quantity (or simply the potential vorticity in the case of a barotropic flow). The extremum in potential vorticity launches inertial-acoustic waves, akin to Rossby waves in planetary atmospheres, and traps modes in its co-rotational singularity (see fig 1 of Meheut et al. 2010). The mechanism was first discussed by Lovelace & Hohlfield (1978) in the context of self-gravitating galactic disks, and mentioned en passant by Toomre (1981), who called them “edge modes”. The instability was discussed again by Papaloizou & Pringle (1984, 1985) in the context of so-called “slender torus” models, hot disks around

quasars modeled locally in radius. The first non-linear numerical simulation of the instability, done by Hawley (1987), found that the trapped non-axisymmetric modes evolved into anticyclonic vortices, but could not follow the calculation until full saturation. The interest on the instability waned after the re-discovery of the magneto-rotational instability (MRI; Velikhov 1959; Chandrasekhar 1960) by Balbus & Hawley (1991) and its rise to paradigmatic status as the source of angular momentum transport and turbulence in disks. The RWI was re-analyzed by Lovelace et al. (1999), who expanded the linear analysis of Papaloizou & Pringle (1984) to non-barotropic disks, and gave the mechanism its modern name. Subsequent work showed that a localized bump in surface density or pressure would cause the instability (Li et al. 2000), and numerical simulations (Li et al. 2001) confirmed its saturation into vortices, with most unstable azimuthal wavenumbers  $m=4-5$ .

Varnière & Tagger (2006) raised the possibility that such surface density jumps would naturally occur at the boundaries between the magnetized and unmagnetized regions of accretion disks. In this boundary, because the unmagnetized region constitutes a “dead zone” to the MRI (Gammie 1996), there exists a transition in turbulent viscosity. The viscous torque at the transition has a component proportional to the negative of the viscosity gradient, so material is accelerated outward in the inner dead zone boundary (negative viscous gradient) and inward in the outer dead zone boundary (positive viscous gradient). This modifies the potential vorticity profile at these transitions, triggering the RWI. Because this component of the viscous torque is also proportional to the shear rate, this process occurs at the shear timescale, not on the much longer viscous timescale.

This two-dimensional scenario, modeling the turbulent transition as jumps in alpha-viscosity (Shakura & Sunyaev 1973) was used by Inaba & Barge (2006) to argue for accumulation of particles in that region, and by Lyra et al. (2008b, 2009) to demonstrate their collapse into planets. The test of this scenario in three-dimensional, magneto-hydrodynamical calculations has yet to be performed. That is the goal of this paper.

In particular, we focus on three questions. First, whether the RWI will drive angular momentum transport. Previous works (Fleming & Stone 2003; Oishi & Mac Low 2009) show that although turbulence in the active upper layers drives waves that propagate into the dead zone, the amount of stress generated is too low to drive significant angular momentum transport, due to the low inertia of the upper active layers. In this work we investigate the effect of a radial, not vertical, resistive transition. As in the midplane the densities are much higher, perhaps the degree of angular momentum transport changes significantly. Moreover, strong anti-cyclonic vortices provide an exciting possibility. Vorticity generates spiral density waves (Heinemann & Papaloizou 2009a,b, 2012) that would have the right velocity correlation to transport angular momentum outwards. It has been shown in local models of unmagnetized disks that by radiation of waves, vortices can maintain a relatively high accretion rate, at

the level of  $\alpha = 10^{-3}$  (Lesur & Papaloizou 2009; Lyra & Klahr 2011). Varnière & Tagger (2006) showed proof-of-concept alpha-disk models that the dead zone can be “revived” by vortices excited in the active/dead boundary, but that still has to be confirmed by MHD simulations.

The second question pertains to the width of the transition. Lyra et al. (2009; see also Regály et al. 2012) show that the maximum width where one expects a pressure bump to trigger the RWI is  $2H$ , where  $H$  is the pressure scale height. The outer edge of the dead zone undergoes a gradual transition, where the density falls monotonically, until the point that it gets so thin that ionizing agents (stellar X-rays or external cosmic rays) can penetrate all the way to the midplane. As this transition should be very smooth, extending through tens of AU, we can exclude that as a possible location for RWI excitation. The inner edge, on the other hand, houses a more exciting possibility, since there the transition in ionization is sharp, set by the collisional ionization of potassium, that occurs at  $\approx 900$  K (e.g. Umebayashi 1983; Turner & Drake 2009).

The other question is whether the magnetic field would in any way inhibit the growth of the RWI. Dzyurkevich et al. (2010) find that a density bump develops at the inner edge of the dead zone, but in the timespan of their simulation, no appreciable growth of non-axisymmetric modes is observed. The same negative result is found in the models of Kato et al. (2009, 2010, 2012) who model inhomogeneous MRI, mimicking the effects of a dead zone. This is curious, since non-axisymmetric modes trapped in the pressure bump should develop counter-rotation, as the fluid element ahead of the bump is accelerated, and the fluid element behind it is decelerated (Hawley 1987). These negative results could be due to the limited azimuthal extent modeled by both works ( $\pi/4$  by Dzyurkevich et al. 2010, local box in the works of Kato et al.), of stratification in the case of Dzyurkevich et al. (2010), or inhibition by the magnetic field.

Although vortices have been reported in MRI-active disks (Fromang & Nelson 2005), the magneto-elliptic instability (Mizerski & Bajer 2009; Mizerski & Lyra 2012) was shown by Lyra & Klahr (2011) to be powerful enough to disrupt vortices otherwise stable in non-magnetized environments. In this work we present models where the dead zone is modeled by a resistive jump in a magnetized disk, and show that the RWI is excited at the dead side of the transition, leading to a giant vortex that survives until the end of the simulation. The paper is organized as follows. In Sect 2 we present the model equations, and in Sect 3 the initial conditions. The results are shown in Sect 4, followed by a discussion and conclusions in Sect 5.

## 2. THE MODEL

### 2.1. Dynamical equations

We perform three-dimensional MHD simulations in the cylindrical approximation, i.e., neglecting the disk vertical stratification and switching off gravity in that direction. The equations solved are

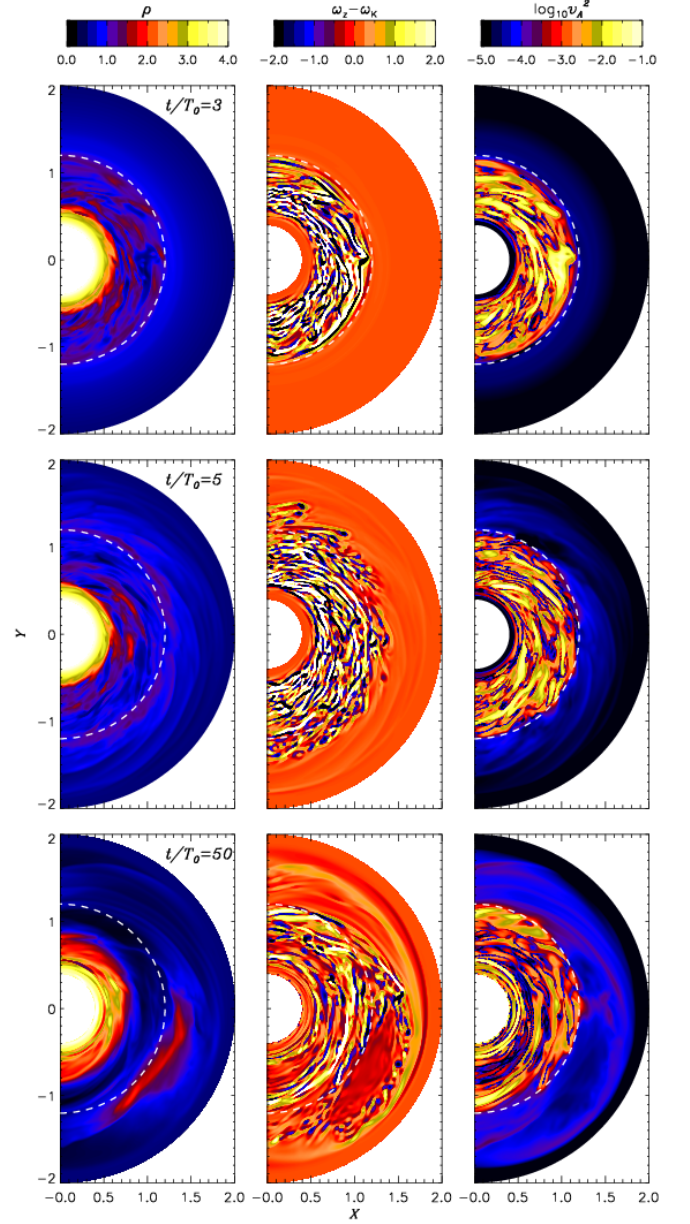


FIG. 1.— Snapshots of density (left), residual vorticity (middle) and Alfvén speed (right) at the midplane in selected times at 3, 5 and 50 reference orbits.

$$\frac{\partial \rho}{\partial t} = -(\mathbf{u} \cdot \nabla) \rho - \rho \nabla \cdot \mathbf{u}, \quad (1)$$

$$\frac{\partial \mathbf{u}}{\partial t} = -(\mathbf{u} \cdot \nabla) \mathbf{u} - \frac{1}{\rho} \nabla p - \nabla \Phi + \frac{\mathbf{J} \times \mathbf{B}}{\rho}, \quad (2)$$

$$\frac{\partial \mathbf{A}}{\partial t} = \mathbf{u} \times \mathbf{B} - \eta \mu_0 \mathbf{J} \quad (3)$$

$$p = \rho c_s^2. \quad (4)$$

where  $\rho$  is the density,  $\mathbf{u}$  the velocity,  $\mathbf{A}$  is the magnetic potential,  $\mathbf{B} = \nabla \times \mathbf{A}$  is the magnetic field,  $\mathbf{J} =$

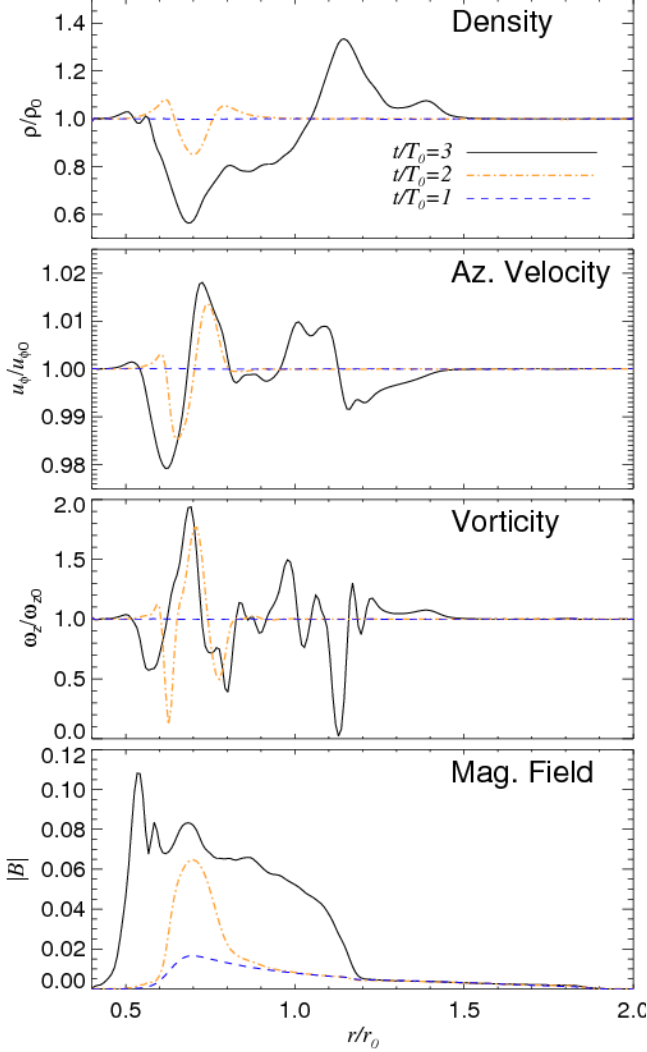


FIG. 2.— Vertical and azimuthal averages of density, azimuthal velocity, vorticity, and magnetic field strength at 1, 2, and 3 orbits, i.e., during linear growth of the MRI. The build-up of magnetic stress at the resistive transition at  $r_\eta = 1.2$  gives rise to an inversion in azimuthal velocity, with super-Keplerian motion inwards and sub-Keplerian motion outwards, generating a dip in potential vorticity. The opposite occurs in the artificial peak of magnetic pressure at  $r = 0.7$  coded in the initial condition, leading to a peak in potential vorticity. Both locations fulfill the conditions for triggering the RWI.

$\mu_0^{-1} \nabla \times \mathbf{B}$  is the current density, and  $p$  is the pressure. The equation of state is locally isothermal. The gravitational potential  $\Phi = -GM_\star/r$  where  $G$  is the gravitational potential,  $M_\star$  is the stellar mass, and  $r$  is the cylindrical radius. The resistivity is a radial function of position. We use a smooth step function

$$\eta(r) = \frac{\eta_0}{2} \left[ 1 + \tanh \left( \frac{r - r_\eta}{\Delta r} \right) \right], \quad (5)$$

in order to mimic the effect of a dead zone. The resistivity passes from  $\eta_0$  to zero over a width  $\Delta r$  centered at an arbitrarily chosen distance  $r_\eta$ .

We solve the equations with the PENCIL CODE <sup>5</sup>

<sup>5</sup> The code, including improvements done for the present work, is

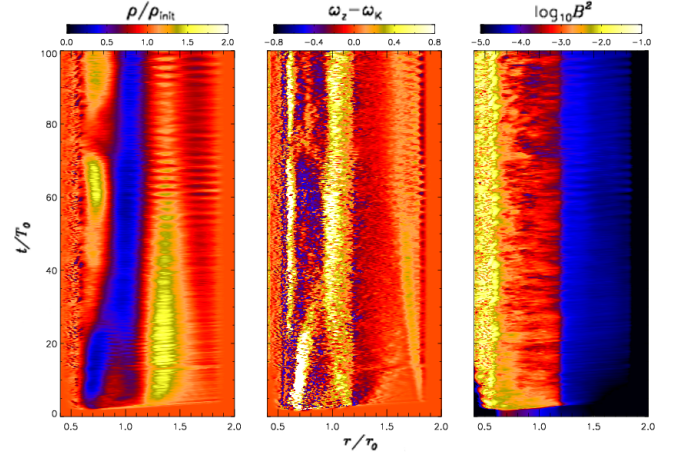


FIG. 3.— Time evolution of the  $\phi$ -z averaged ( $r$ -dependent) density (left panel), vertical vorticity (middle panel) and magnetic energy (right panel) for the fiducial model. A density enhancement is seen at the dead side of the resistive transition at  $r = 1.2$ , matching radial locations of lower vorticity. Curiously, other vortices are excited in the active zone. One exists at  $r \approx 0.7$  from  $t \approx 3T_0$  to  $t \approx 20T_0$ , and another next to the inner boundary from  $t \approx 40T_0$  to  $t \approx 70T_0$ , after which it decays and restarts at  $t \approx 85T_0$ .

which integrates the evolution equations with sixth order spatial derivatives, and a third order Runge-Kutta time integrator. Sixth-order hyper-dissipation terms are added to Eq. (1)-Eq. (3), to provide extra dissipation near the grid scale, explained in Lyra et al. (2008a). They are needed because the high order scheme of the Pencil Code has little overall numerical dissipation (McNally et al. 2012).

## 2.2. Initial Conditions

We model a three-dimensional disk on a uniformly spaced mesh in cylindrical coordinates  $(r, \phi, z)$ , ranging over  $r=[0.4, 2.0]r_0$  and  $z=[-0.1, 0.1]r_0$ , where  $r_0$  is a reference radius. We run models with azimuthal coverage  $L_\phi = \pi$  and  $L_\phi = 2\pi$ . The fiducial model with  $L_\phi = \pi$  has resolution  $[N_r, N_\phi, N_z] = [192, 384, 64]$ .

The density and sound speed are set as radial power-laws

$$\rho = \rho_0 \left( \frac{r}{r_0} \right)^{-q_\rho}; \quad c_s^2 = c_{s0}^2 \left( \frac{r}{r_0} \right)^{-q_T} \quad (6)$$

with  $q_\rho = 1.5$  and  $q_T = 1.0$ . The initial angular velocity profile is corrected by the thermal pressure gradient

$$\dot{\phi}^2 = \Omega^2 + \frac{1}{r\rho} \frac{\partial p}{\partial r} \quad (7)$$

where  $\Omega = \Omega_0 (r/r_0)^{-q}$  with  $q = 1.5$  is the Keplerian angular velocity.

The magnetic field is set as a net vertical field, with four MRI wavelengths resolved in the vertical range. The constraint  $\lambda_{\text{MRI}} = 2\pi v_A \Omega^{-1} = L_z/4$  translates into a radially varying field

publicly available under a GNU open source license and can be downloaded at <http://www.nordita.org/software/pencil-code>

$$v_A = \frac{L_z \Omega}{8\pi} \sqrt{\mu_0 \rho} = v_{A0} \left( \frac{r}{r_0} \right)^{-(q+q_\rho/2)}, \quad (8)$$

i.e., a field falling as a 9/4 power-law. We use units such that

$$GM_\star = r_0 = \rho_0 = \mu_0 = 1 \quad (9)$$

and omit these factors hereafter. Thus,  $v_{A0} \approx 8 \times 10^{-3}$  in code units. The reference sound speed is set at  $c_{s0}=0.1$ . The dimensionless plasma beta parameter  $\beta = 2c_s^2/v_A^2$  then ranges from 50 in the inner disk to 1250 in the outer. Noise is added to the velocities at the  $10^{-4}$  level. In this configuration, the MRI grows and saturates quickly in 3 local orbits. We apply the noise and the magnetic field only in the radial range  $r=[0.6,1.8]$  to avoid growth of the instability near the boundaries. We use reflective boundaries, with a buffer zone of width 0.2 at each radial border, that drives the quantities to the initial condition on a dynamical timescale.

In the presence of resistivity, the excitation of the MRI is controlled by the Elsässer number

$$\Lambda = \frac{\lambda v_A}{\eta}, \quad (10)$$

which is the magnetic Reynolds number with velocity equal to the Alfvén speed, and  $\lambda$  the relevant magnetic length scale. We set the reference resistivity  $\eta_0$  so that the Elsässer number of the largest wavelength present in the box (i.e.,  $\lambda = L_z$ ) is unity at  $r_0$ , thus quenching the MRI outward of that radius. This constraint translates into  $\eta_0 = L_z v_{A0} = 1.6 \times 10^{-3}$ . We place the resistivity jump at  $r_\eta=1.2$ , so that at that location  $\Lambda = 0.75 < 1$ .

### 3. RESULTS

#### 3.1. Fiducial model

The fiducial model ranges  $\pi$  in azimuth, with a resolution of  $[N_r, N_\phi, N_z]=[192, 384, 64]$ , and a sharp resistivity transition at  $r_\eta = 1.2$  of width  $\Delta r = 10^{-2}$ . The MRI starts from the inner disk and quickly saturates in 3 local orbits. We show in Fig. 1 the state of the disk for density (left panels), residual vertical vorticity (vertical vorticity minus the vertical Keplerian vorticity, middle panels) and Alfvén speed (right panels) in selected snapshots. The dashed line marks the boundary between MRI-active and dead zones. We see that the magnetic energy is well confined to the active zone, with only some very minor diffusion into the dead zone. The turbulence in the active zone propagates spiral density waves into the dead zone as seen in the snapshots at  $t/T_0 = 5$  (where  $T_0 = 2\pi$  is the orbital period at  $r_0$ ).

In Fig. 2 we show that the conditions for the development of the RWI are fulfilled in this disk model. We plot the azimuthal and vertical averages as a function of radius of density, azimuthal velocity, vorticity, and magnetic field, for the first three orbits. In a barotropic disk, an extremum in potential vorticity  $\omega_z/\rho$  will launch the RWI (Lovelace et al. 1999). This condition is brought about by the transition in magnetic pressure near  $r_\eta$ .

At later times (lower panels of Fig. 1), a giant vortex is seen on the dead side of the transition. The density

enhancement (lower left) matches spatially a vorticity minimum, confirming its anticyclonic nature.

We show in Fig. 3 the time evolution of the azimuthal and vertical averages of the same quantities shown in Fig. 1. In the density plot we see the vortex as an enhancement at the dead size of  $r_\eta$ . It weakens with time but attains a steady state after  $t/T_0=60$ . The vorticity plot shows that the density enhancement is traced by anticyclonic vorticity. Conversely the density dips are spatially correlated with regions of cyclonic vorticity. Though the resistivity impedes the growth of the MRI in the dead zone, it experiences diffusion of some magnetic field from the active zone. It thus appears weakly magnetized instead of completely demagnetized.

Interestingly, in the same plots we see that vortices are excited in the magnetized regions. A weak vortex is seen in the middle of the active zone at very early times,  $t/T_0 < 5$ . It eventually decays, after 20 orbits. Other intermittent vortices are also seen to be excited, at  $r=0.7$ , between 40 and 70 orbits, and again after 85 orbits. These vortices exist in the midst of MRI turbulence, as in the models of Fromang & Nelson (2005). Strictly speaking, Lyra & Klahr (2011) state that vortices that are excited by the baroclinic instability and survive in hydrodynamical models are destroyed when a magnetic field is abruptly introduced in the simulation. They do not exclude excitation of MHD vortices by other ways. Still, these magnetized vortices should host magneto-elliptic instabilities (Mizerski & Bajer 2009; Mizerski & Lyra 2012), and given their strength, should not exist; unless vorticity injection by the RWI is faster than destruction by the magneto-elliptic instability in the relevant scales.

The origin of the vortex at  $r=0.7$  lies in the initial condition, because we used a field with a peak in magnetic pressure around that radius. This is seen in Fig. 2 as the peak in magnetic pressure translates into an azimuthal velocity inversion and a peak of potential vorticity. This incurs a non-equilibrium configuration, that induces sub-Keplerian motion inwards of the peak, and super-Keplerian motion outwards. It triggers a localized zonal flow, that in turns excites the non-axisymmetric modes of the RWI.

#### 3.2. Angular momentum transport

We display in Fig. 4 the measured Maxwell and Reynolds stresses. The Reynolds stress is shown for both the active and dead zone. We see that the Maxwell and Reynolds stresses in the active zone reach the  $10^{-2}$  level, agreeing with previous studies (Papaloizou & Nelson 2003; Fromang & Nelson 2006; Lyra et al. 2008a; Dzyurkevich et al. 2010; Beckwith et al. 2011; Flock et al. 2011; Sorathia et al. 2012). The novel result of our model is that the Reynolds stress in the dead zone is also at the  $10^{-2}$  level, only slightly lower than in the active zone.

Without viscous dissipation, the angular momentum is transported to the outer boundary, where it is damped, while the matter accretes. As a result of outward angular momentum transport, the vortex should migrate inwards (Paardekooper et al. 2010; Lyra & Klahr 2011) However, this is not observed in the simulations. The vortex keeps radiating waves, yet it sits in the pressure maximum that generated it, which acts as a migra-



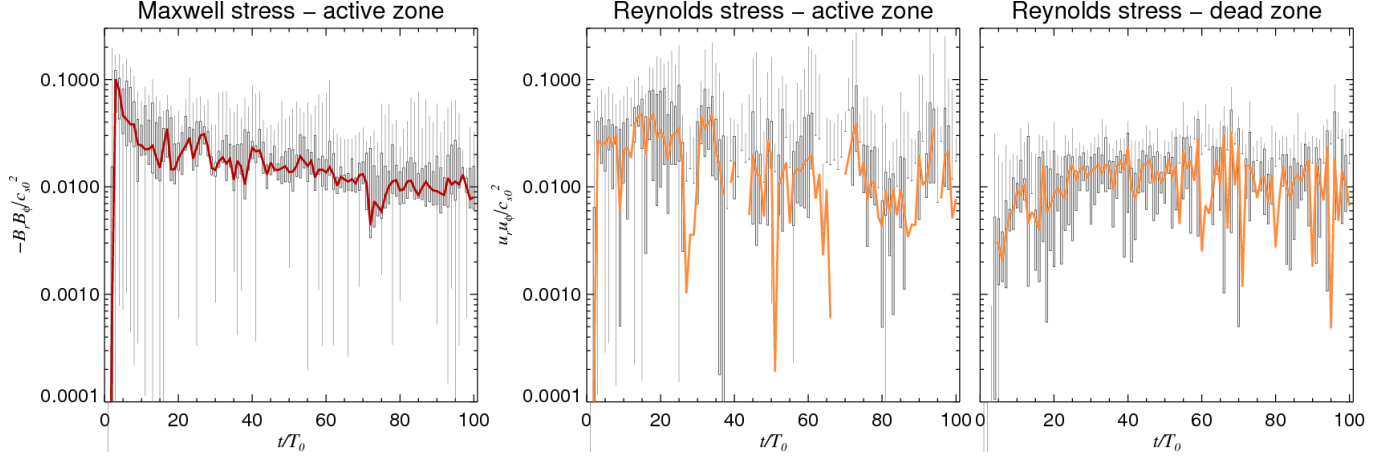


FIG. 4.— Maxwell and Reynolds stresses as a function of time in the active and dead zones. Measurements were taken every  $T_0 = 2\pi$ , and shown in the plot as box-and-whiskers five point summaries. The light thin grey lines are the whiskers marking the minimum and maximum values, the dark grey thick lines marks the lower and upper quartiles that box 50% of the values. A thicker colored line traces the median. High levels of Reynolds stress are maintained in the dead zone by the spiral density waves excited by the vortex at the active/dead boundary.

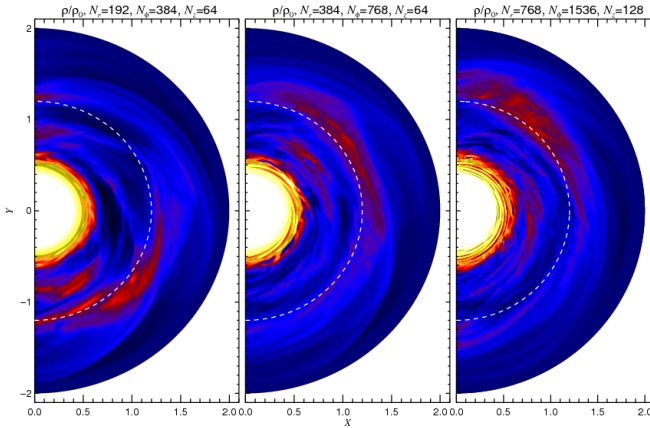


FIG. 5.— Models of resolution  $192 \times 384$ ,  $384 \times 768$  and  $768 \times 1536$  in the midplane. The vertical resolution is 64 in the first two plots, and 128 in the last one. The vortex in the magnetized zone, that should be unstable, shrinks in size with increasing resolution, but is not quenched even in the highest resolution model (see text). The outer vortex exists in the dead zone and is not subject to the same destabilizing mechanism. The same colorbar is used as in Fig. 1.

tion barrier. The same is seen in the models of Meheut et al. (2010, 2012b).

### 3.3. Resolution study

According to the results of Lyra & Klahr (2011), the magneto-elliptic instability should not allow the formation of the vortices seen in the MRI-active region. This suggests that the models presented are under-resolving the MEI-modes. To examine this possibility, we run models with twice ( $N_r = 384$ ,  $N_\phi = 768$ ,  $N_z = 64$ ) and four times ( $N_r = 768$ ,  $N_\phi = 1536$ ,  $N_z = 128$ ) the midplane resolution of the fiducial model. The flow pattern after 12 orbits is shown in Fig. 5. We see that the inner vortex in the magnetized region has shrunk in size while the outer one in the dead zone has not. This is evidence that the MEI is being excited, and the vortex core shrinks to a size where it is under-resolved. The size of the scale height in all models is  $H = hr = 0.1r$ , so  $H=0.08$  for the

location of the inner vortex. The low resolution model resolves that scale with  $H/\Delta r=9$  points, the middle resolution one with 19 points and the highest resolution model with 38 points.

We see that even in the highest resolution model, the density enhancement persists. We conclude that this vortex is either magnetically stable (which is problematic in view of the claims of Lyra & Klahr 2011) or the resolution requirement to capture the unstable modes has not been met. As we could not push the resolution even further (the highest resolution model already consumed 2 million computer hours), the question of the stability of the inner vortex will be addressed in a future work, in local box models, to satisfy the resolution requirement.

### 3.4. $2\pi$ model

As shown by Flock et al. (2011) the main features of the MRI can be captured with a domain spanning  $\pi$  in azimuth as well as they can in a domain spanning  $2\pi$ . That statement, however, though applying for the axisymmetric MRI, does not automatically apply to the non-axisymmetric RWI, for which the most unstable wavelengths are  $m = 4$  and  $m = 5$  (Li et al. 2000). Viscous mergings then transfer the power towards lower wavenumbers, in a cascade leading to  $m = 1$ , i.e., a single vortex<sup>6</sup>.

We check if there are significant differences pertaining to azimuthal domain size by performing a simulation spanning  $2\pi$  radians and comparing the result with the fiducial model. The model has the same numerical resolution, using twice the grid points in  $\phi$ ,  $[N_r, N_\phi, N_z] = [192, 768, 64]$ . The comparison is shown in Fig. 6. It is seen that at 12 orbits the  $2\pi$  model shows a conspicuous  $m=2$  mode, whereas the  $\pi$  model contains a single vortex at the same time. The two vortices in the  $2\pi$  model later merge into a  $m = 1$  mode, and as a result

<sup>6</sup> The  $m = 1$  mode can cascade further, back to  $m = 0$ , thus turning the RWI into a cycle (see Regály et al. 2012). However, this development occurs only over long evolution times and will not be dealt with in this work.

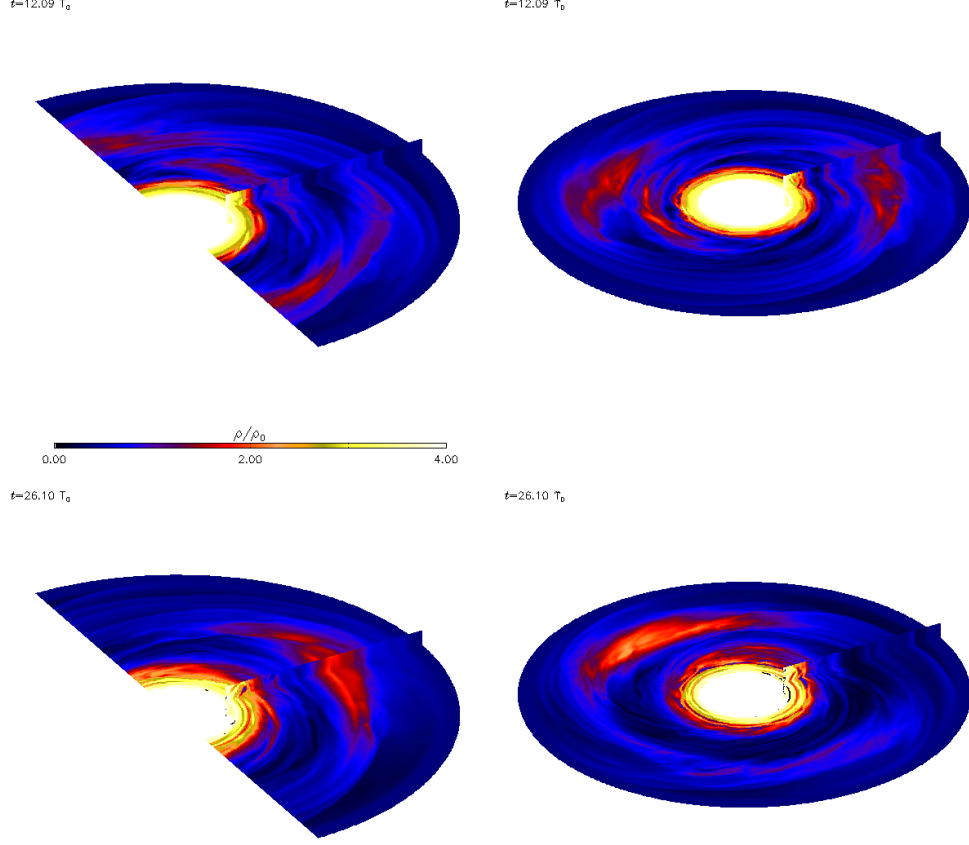


FIG. 6.— Since the RWI is non-axisymmetric, we assess the influence of azimuthal domain size  $L_\phi$  on its evolution by comparing models of  $L_\phi = \pi$  (left panels) and  $L_\phi = 2\pi$  (right panels). Upper panels show the models at 12 orbits, lower panels at 26 orbits. Despite differences at early times (at 12 orbits the vortex cascade is still at  $m = 2$  in the  $2\pi$  models), once the inverse cascade is complete and a single vortex survives, the models look remarkably similar.

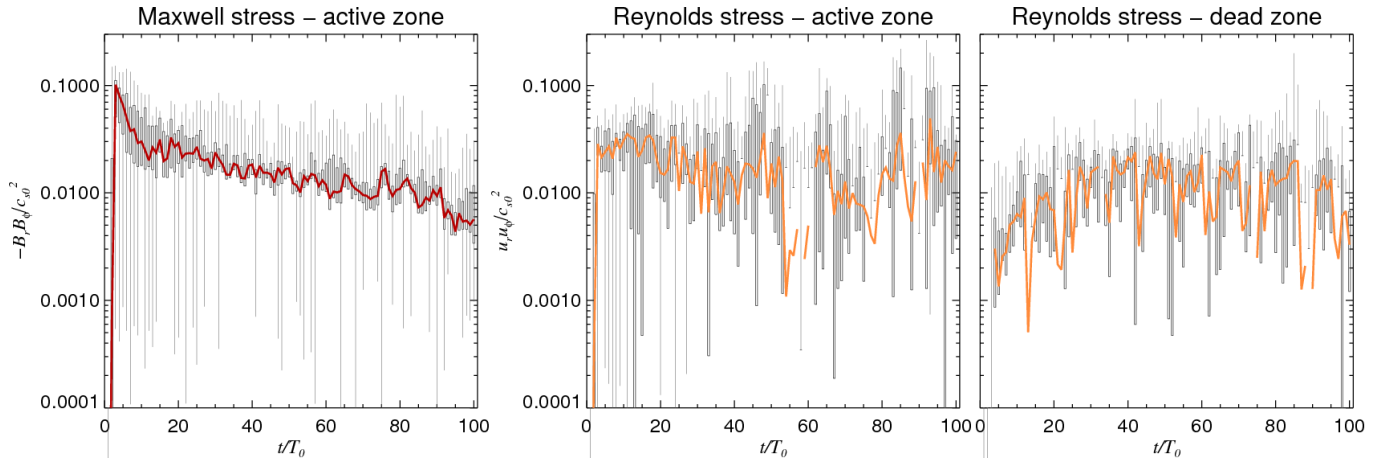


FIG. 7.— Same as Fig. 4 but for the full  $2\pi$  model. The level of angular momentum transport is very similar to the model spanning only  $\pi$  in azimuth. We conclude that the latter model leaves enough azimuthal room to avoid vortex self-interaction across the periodic boundary.

the flows in both cases are very similar at  $t=26$  orbits.

We also measure the angular momentum transport in the  $2\pi$  model, shown in Fig. 7. The stresses are very similar to the ones shown in Fig. 4, for the  $\pi$  model. This means a box size of  $L_\phi=\pi$  already provides enough azimuthal spacing so that the vortex does not interact with itself in a way that significantly affects the stresses (the same is not true for local boxes).

We conclude that studies concerning the linear growth of the instability require full  $2\pi$  simulations, yet  $\pi$  suffices if the interest is in the saturated,  $m=1$ , state.

#### 4. CONCLUSIONS

We performed the first simulation of a RWI-unstable boundary between dead and active zones in a protoplanetary disk with 3D resistive-magnetohydrodynamical models. We use a sharp resistive transition, that should be characteristic of the inner dead zone boundary.

We find that Rossby vortices are excited on the dead side of the transition. They first appear in an  $m=4$  mode, as expected from the RWI, then quickly merge viscously into a  $m=2$  mode, and finally reach  $m=1$ , becoming a single giant vortex immediately outside of the transition. This lends credence to previous works that relied on alpha disk models with angular velocity transitions to trigger the RWI (Inaba & Barge 2006; Lyra et al. 2008b, 2009; Meheut et al. 2010, 2012b).

We also assess the mass accretion rate in the dead zone, which is a result both of waves propagating from the active zone and of waves radiated by the vortex. We find normalized Reynolds stresses of similar magnitude in both the active and in the dead zones, at the  $10^{-2}$  level. Vortex-free transitions develop dead zone stresses two orders of magnitude quieter than the active zones, so this high accretion rate is a manifestation of the ability of the vortex to maintain high accretion rates. The same level is found for angular momentum transport in baroclinically unstable local disk models (Lesur & Papaloizou 2009; Lyra & Klahr 2011). Because the vortex is born in a high pressure ridge, it does not migrate further in; the ridge acts as a migration barrier.

A puzzling aspect of our model is the development of a weak vortex in the middle of the active zone. The vortex was driven by the RWI at the peak in magnetic pressure due to the artificial initial condition. Yet according to a recent study by Lyra & Klahr (2011), rotating magnetized vortices should be host to a set of

unstable centrifugal hydromagnetic modes (magneto-elliptic instability) that should ultimately break closed elliptic streamlines. If that is the case, then our models are either under-resolving these modes, or vorticity injection by the RWI is faster than destruction by the magneto-elliptic instability. We pushed the resolution of the global model to the limit allowed by current computational power. The vortex shrank with increasing resolution, but we could not quench it completely. A conclusive test will require local models, which we plan to undertake in future work. A study of convergence with dead zone size, and an assessment of how wide the resistive jump can be while still allowing for Rossby vortex excitation are also lacking.

The models presented leave room for exciting developments. First, we used a static resistivity profile. Though this is shown by Latter & Balbus (2012) to produce acceptable results, we plan to include dynamic resistivity in future models, following the reduced recombination network of Ilgner & Nelson (2006a,b,c), used by Turner & Sano (2008); Turner & Drake (2009); Gressel et al. (2011); Hirose & Turner (2011) and Gressel et al. (2012). Effects of Hall MHD and ambipolar diffusion (Wardle 1999; Salmeron & Wardle 2005; Bai & Stone 2011; Bai 2011) may also impact significantly on the nature of the active/dead radial transition. Future work will also include stratification, shown through numerical (Meheut et al. 2010, 2012b) and analytical work (Meheut et al. 2012a; Lin 2012) to matter significantly for the internal dynamics of 3D vortices. Finally, interacting particles should be included to assess the ability of three-dimensional Rossby vortices in dead zones to assist on planet formation.

The writing of this paper was started at the American Museum of Natural History with financial support by the National Science Foundation under grant no. AST10-09802, and completed at the Jet Propulsion Laboratory, California Institute of Technology, under a contract with the National Aeronautics and Space Administration. This work was performed under allocation TG-MCA99S024 from the Extreme Science and Engineering Discovery Environment (XSEDE), which is supported by National Science Foundation grant number OCI-105357. The computations were performed on the Kraken system at the National Institute for Computational Sciences. We thank the anonymous referee for useful suggestions.

#### REFERENCES

- Adams, F. C. & Watkins, R. 1995, *ApJ*, 451, 314  
 Bai, X.-N. & Stone, J. 2011, *ApJ*, 739, 50  
 Bai X.-N. 2011, *ApJ*, 739, 51  
 Balbus, S. & Hawley, J. 1991, *ApJ*, 376, 214  
 Barge, P. & Sommeria, J. 1995, *A&A*, 295, 1  
 Batchelor, G. K. 1969, *PhFl*, 12, 233  
 Bayly, B. J. 1986, *PhRvL*, 57, 2160  
 Beckwith, K., Simon, J. B., Armitage, P. J., 2011, *MNRAS*, 416, 361  
 Bracco, A., Chavanis, P.-H., Provenzale, A., Spiegel, E. A. 1999, *PhFl*, 11, 2280  
 Brauer, F., Dullemond, C. P., & Henning, Th. 2008a, *A&A*, 480, 859  
 Cassini, G. D. 1666, cited in *Phil. Trans. Roy. Soc.* 1666, 8, 143 *Of a permanent spot in Jupiter; by which is manifested the conversion of Jupiter about its own axis.* Hutton, C., Shaw, G., & Pearson, R., *Phil. Trans. Roy. Soc.* abridged version 1665-1800, London, 1809.  
 Chandrasekhar, S. 1960, *Proc. Nat. Acad. Sci.*, 46, 253  
 Chandrasekhar, S. 1961, *Hydrodynamic and Hydromagnetic Stability* (Oxford: Clarendon), 384  
 Chang, P. & Oishi, J. 2010, *ApJ*, 721, 1593  
 Cuzzi, J. N., Hogan, R. C., & Shariff K. 2008, *ApJ*, 687, 1432  
 Dzyurkevich, N., Flock, M., Turner, N. J., Klahr, H., & Henning, Th. 2010, *A&A*, 515, 70  
 Falorni, M. 1987, *JBAA*, 97, 215  
 Fleming, T. & Stone, J. 2003, *ApJ*, 585, 908  
 Flock M., Dzyurkevich, N., Klahr, H., Turner, N. J., & Henning, Th. 2011, *ApJ*, 735, 122  
 Fromang, S. & Nelson, R. P. 2005, *MNRAS*, 364, 81  
 Fromang, S. & Nelson, R. P. 2006, *A&A*, 457, 343  
 Gammie, C. F. 1996, *ApJ*, 457, 355  
 Godon & Livio 1999, *ApJ*, 523, 350  
 Godon & Livio 2000, *ApJ*, 537, 396



- Goldreich, P. & Ward, W. R. 1973, *ApJ*, 183, 1051
- Gressel, O., Nelson, R. P., & Turner, N. J. 2012, *MNRAS*, 2714
- Gressel, O., Nelson, R. P., & Turner, N. J. 2012, *MNRAS*, 415, 3291
- Haghighipour, N. & Boss, A. P. 2003, *ApJ*, 583, 996
- Hawley, J. F. 1987, *MNRAS*, 225, 677
- Heinemann, T. & Papaloizou, J. C. B. 2012, *MNRAS*, 419, 1085
- Heinemann, T. & Papaloizou, J. C. B. 2009, *MNRAS*, 397, 64
- Heinemann, T. & Papaloizou, J. C. B. 2009, *MNRAS*, 397, 52
- Hirose, S. & Turner, N. J. 2011, *ApJ*, 732, 30
- Hooke, R. 1665, cited in *Phil. Trans. Roy. Soc.* 1665, 1, 3 *A spot in one of the belts of Jupiter*. Hutton, C., Shaw, G., & Pearson, R., *Phil. Trans. Roy. Soc.* abridged version 1665-1800, London, 1809.
- Ilgner, M. & Nelson, R. P. 2006, *A&A*, 445, 731
- Ilgner, M. & Nelson, R. P. 2006, *A&A*, 445, 223
- Ilgner, M. & Nelson, R. P. 2006, *A&A*, 445, 205
- Inaba, S. & Barge, P. 2006, *ApJ*, 649, 415
- Johansen, A., Youdin, A., & Klahr, H. 2009, *ApJ*, 697, 1269
- Johansen, A., Oishi, J. S., Mac Low, M.-M., Klahr, H., Henning, Th., & Youdin, A. 2007, *Nature*, 448, 1022
- Johansen, A. & Youdin, A. 2007, *ApJ*, 662, 627
- Johansen, A., Andersen, A. C., & Brandenburg, A. 2004, 417, 361
- Kato, M. T., Fujimoto, M., & Ida, S. 2012, *ApJ*, 747, 11
- Kato, M. T., Fujimoto, M., & Ida, S. 2012, *ApJ*, 714, 1155
- Kato, M. T., Nakamura, K., Todoroko, R., Fujimoto, M., & Ida, S. 2009, *ApJ*, 691, 1697
- Kerswell, R. R. 2002, *AnRFM*, 34, 83
- Klahr, H. 2006, *ApJ*, 639, 432
- Klahr, H. 2004, *ApJ*, 606, 1070
- Klahr, H. & Bodenheimer, P. 2003, *ApJ*, 582, 869
- Latter, H. N. & Balbus, S. 2012, arXiv:1203.6572
- Lesur, G. & Papaloizou, J. C. B. 2009, *A&A*, 498, 1
- Li, H., Finn, J. M., Lovelace, R. V. E., & Colgate, S. A. 2000, *ApJ*, 533, 1023
- Li, H., Colgate, S. A., Wendroff, B., & Liska, R. 2011, *ApJ*, 551, 874
- Lin, M.-K. 2012, arXiv:1203.2630
- Lovelace, R. V. E., Li, H., Colgate, S. A., & Nelson, A. F. 1999, *ApJ*, 513, 805
- Lovelace, R. V. E. & Hohlfield, R. G. 1978, *ApJ*, 221, 51
- Lyra, W. & Klahr, H. 2011, *A&A*, 527A, 138
- Lyra, W.; Johansen, A.; Zsom, A.; Klahr, H.; Piskunov, N. 2009, *A&A*, 497, 869
- Lyra, W., Johansen, A., Klahr, H., & Piskunov, N. 2008, *A&A*, 491, L41
- Lyra, W., Johansen, A., Klahr, H., & Piskunov, N. 2008, *A&A*, 479, 883
- Lytton, R. A. 1972, *MNRAS*, 160, 255
- Marcus, P. S. 1993, *ARA&A*, 31, 523
- McNally, C. P., Lyra, W., & Passy, J.-C. 2012, arXiv:1111.1764
- Méheut, H., Casse, F., Varnière, P., & Tagger M. 2010, *A&A*, 516, 31
- Méheut H., Cong, Y., & Lai, D. 2012, *MNRAS*, 2748
- Méheut H., Keppens, R., Casse, F., & Benz, W. 2012, arXiv:1204.4390
- Mizerski, K. A. & Bajer, K. 2009, *JFM*, 632, 401
- Mizerski, K. A. & Lyra, W. 2012, *JFM*, 698, 358
- Oishi, J. S. & Mac Low, M.-M. 2009, *ApJ*, 704, 1239
- Okuzumi, S., Tanaka, H., Kobayashi, H., & Wada K. 2012, arXiv:1204.5035
- Paardekooper, S.-J., Lesur, G., & Papaloizou J. C. B. 2010, *ApJ*, 725, 146
- Pan, L., Padoan, P., Scalo, J., Kritsuk, A. G., & Norman, M. L. 2011, *ApJ*, 740, 6
- Papaloizou, J. C. B. & Pringle, J. E. 1984, *MNRAS*, 208, 721
- Papaloizou, J. C. B. & Pringle, J. E. 1985, *MNRAS*, 213, 799
- Papaloizou, J. C. B. & Nelson, R. P. 2003, *MNRAS*, 339, 983
- Pierrehumbert, R. T. 1986, *PhRvL*, 57, 2157
- Regály, Zs., Juhász, A., Sándor, Zs., & Dullemond, C. P. 2012, *MNRAS*, 419, 1701
- Safronov, V. S. 1969, *Evolutsiia Doplanetnogo Oblaka* (English transl: *Evolution of the Protoplanetary Cloud and Formation of Earth and the Planets*, NASA Tech. Trans. F-677, Jerusalem: Israel Sci. Transl., 1972)
- Salmeron, R. & Wardle, M. 2005, *MNRAS*, 361, 45
- Shakura, N. I. & Sunyaev, R. A. 1973, *A&A*, 24, 337
- Simon, J. B., Beckwith, K., & Armitage, P. J. 2012 *MNRAS*, 2808
- Sorathia, K. A., Reynolds, C. S., Stone, J. M., & Beckwith, K. 2012, *ApJ*, 749, 189
- Strutt, J. W. 1916, *Proc. Roy. Soc.* 93, 148. *Scientific Papers by John William Strutt, Baron Rayleigh. Vol. 6: 1911-1919*, Cambridge University Press, 1920.
- Strutt, J. W. 1880, *Proc. Lond. Maths. Soc.* 11, 57. *Scientific Papers by John William Strutt, Baron Rayleigh. Vol. 1: 1869-1881*, Cambridge University Press, 1920.
- Tanga P., Babiano, A., Dubrulle, B., & Provenzale, A. 1996, *Icarus*, 121, 158
- Toomre, A. 1981, What amplifies the spirals. In *The Structure and Evolution of Normal Galaxies*, Proceedings of the Advanced Study Institute, Cambridge, England, Cambridge and New York, Cambridge University Press, 1981, p.111-136.
- Turner, N. J. & Drake, J. F. 2009, *ApJ*, 703, 2152
- Turner, N. J. & Sano, T. 2008, *ApJ*, 679, 131
- Umebayashi, T. 1983, *PThPh*, 69, 480
- Umurhan O. M. 2010, *A&A*, 521, 25
- Varnière, P. & Tagger, M. 2006, *A&A*, 446, 13
- Velikhov, E. P. 1959, *Soviet Phys. JETP*, 36, 1398
- Youdin, A. & Johansen A. 2007, *ApJ*, 662, 613
- Youdin, A. N. & Goodman, J. 2005, *ApJ*, 620, 459
- Youdin, A. N. & Shu, F. H. 2002, *ApJ*, 580, 494
- Wardle, M. 1999, *MNRAS*, 307, 849
- Weidenschilling, S.J. 1977, *MNRAS*, 180, 57